Vladimir Stevanović

Professor

Sanja Prica

Research Assistant

Blaženka Maslovarić

Research Assistant

University of Belgrade
Faculty of Mechanical Engineering

Multi-Fluid Model Predictions of Gas-Liquid Two-Phase Flows in Vertical Tubes

A consistent one-dimensional multi-fluid model is developed for the prediction of two-phase flows in vertical pipes. The model is based on the mass, momentum and energy balance equations for every fluid stream involved in the observed two-phase flow pattern, and corresponding closure laws for interface transfer processes. The steady-state balance equations are transformed in a form suitable for a direct application of the numerical integration method for the system of ordinary differential equations. Thermal-hydraulic processes along the whole length of the boiling channel are simulated, from the flow and heating of subcooled liquid at the flow channel inlet, and up to the liquid film dry out and gas-entrained droplets mist flow at the outlet. Also, the model is tested against several partial effects of two-phase flow.

Keywords: Two-phase flow, Numerical simulation, Vertical tubes

1. INTRODUCTION

Gas and liquid phase two-phase flows in vertical tubes are encountered in various types of steam generators, heat exchangers and condensers [23]. The prediction of two-phase flow parameters is important in design and in operational and safety analyses of this equipment.

Typical two-phase flow patterns in the vertical evaporation channel are presented in Fig. 1. One phase liquid flow exists at the tube inlet. A formation of the bubbles at the heated wall, while the bulk liquid is still subcooled, is known as the subcooled boiling. The saturated boiling occurs when the liquid phase reaches saturated conditions determined with the local pressure. The slug and churn flows occur with the increase of vapour volume fraction (void). At high voids the annular flow exists, which transforms towards mist flow upon complete evaporation of liquid film on the heated wall. As presented, a certain flow pattern exists over some channel length, and then transforms into another flow pattern. A transformation from one flow pattern into another can be accompanied by the change of number of streams. Bubbly and churn flow patterns, characterized with two fluid streams-liquid and vapour, transforms into annular flow pattern that have three fluid streams: liquid film on the wall, vapour core and droplets entrained in the vapour stream. Therefore, a two-phase flow in a flow channel is usually characterized by regions which comprise several fluid streams, each of them prevailing over certain channel length. Applying the multi-fluid modelling approach to such flow conditions means that one two-phase flow channel should be described with several multi-fluid

models, where these models are based on the mass, momentum and energy balance equations for each of the fluid streams involved in the two-phase flow, as well as on the corresponding closure laws for the prediction of the gas-liquid and fluid-wall interface transport processes. Mechanistic models are applied for the prediction of flow pattern transitions, various modes of mass, momentum and energy interfacial transfers, such as droplets entrainment or deposition, and boiling under diabatic and adiabatic conditions. In this way, better physical rationalism can be applied to the modelling of these specific processes which are very important for the proper understanding of two-phase flow phenomena and accurate prediction of two-phase flow transport processes. Multi-fluid modelling approach is substantial improvement in comparison to the prevailing application of purely empirically based correlations for two-phase flow phenomena. Therefore, it enables physically based investigation of various two-phase flow phenomena, such as boiling crises, vapour volume fraction, pressure change and frictional pressure drop, critical flow conditions, flooding, etc. The multi-fluid modelling approaches have been applied previously to the prediction of several two-phase flow phenomena, such as droplets entrainment in annular flow [1,12,16,18], the critical heat flux prediction [15,21], and two-phase flow pressure changes [1,12,15,18].

This paper presents general multi-fluid governing equations for up to four fluid streams, together with corresponding closure laws. Each fluid stream is described by mass, momentum and energy balance equation. These governing equations are coupled through closure laws that describe transport processes at the fluids' interfaces. The ability of the model to describe the two-phase flow phenomena is shown by examples of numerical predictions of gas-phase volume fractions in bubbly and transitional churn flows, the boiling crises in vertical upward two-phase flows in pipes, and two-phase critical flows.

single-phase
vapour

dispersed-drop
flow

annular
flow

churn
flow

plug
flow

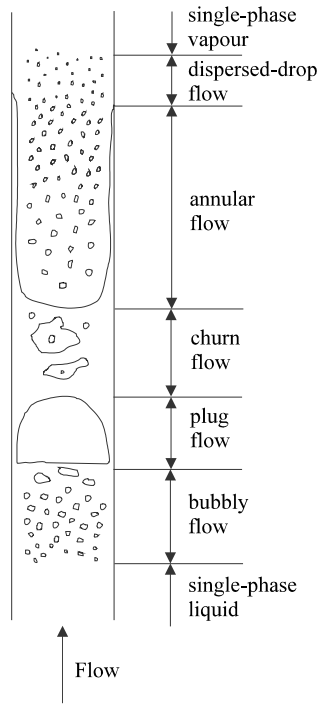bubbly
flow

single-phase
liquid

Flow

Figure 1. Two-phase flow patterns in evaporating channel

2. MULTI-FLUID MODEL DEVELOPMENT

Developed multi-fluid model comprises up to four fluid streams, where the number of fluid streams (n) depends on the simulated two-phase flow pattern. One fluid stream ($n = 1$) is applied to the simplest situation of one-phase flow. Two fluid streams ($n = 2$) are applied to bubbly and transitional (churn or slug) flow patterns, as well as to the mist gas-entrained droplets flow in case of liquid film depletion and wall dry-out in annular flow. Liquid film flow on the wall, vapour flow and droplets entrained in the vapour core are represented by three fluid streams ($n = 3$) for annular flow pattern in a pipe. Four fluid streams ($n = 4$) correspond to the annular flow in annuli, where these streams represent liquid film on the inner wall, liquid film on the outer wall, vapour core and droplets entrained in the vapour stream. Mass, momentum and energy balance equations are written for each fluid stream. Transfer processes at the interfaces of fluid pairs that are in contact, as well as between the fluid streams and the walls are calculated by the closure laws. The balance equations have the following general form for transient one-dimensional flow conditions

2.1 Balance Equations

Mass balance

$$\frac{\partial(\alpha_k \rho_k)}{\partial t} + \frac{\partial(\alpha_k \rho_k u_k)}{\partial x} = M_k \tag{1}$$

Momentum balance

$$\frac{\partial(\alpha_k \rho_k u_k)}{\partial t} + \frac{\partial(\alpha_k \rho_k u_k^2)}{\partial x} + \alpha_k \frac{\partial p}{\partial x} = M_{n+k} \tag{2}$$

Energy balance

$$\frac{\partial(\alpha_k \rho_k h_k)}{\partial t} + \frac{\partial(\alpha_k \rho_k h_k u_k)}{\partial x} = M_{2n+k} \tag{3}$$

where M represents mass, momentum and energy source terms, index $k = 1, \dots n$ denotes the fluid stream and n denotes the total number of fluid streams involved in the simulated two-phase flow pattern. The source terms on the right hand side of Eqs. (1-3) depend on the modelled two-phase flow pattern. They are presented, as an example, for the bubbly and transitional flow regimes in Table 1. The above balance equations are completed with the following volume balance

Volume fraction balance

$$\sum_{k=1}^{n} \alpha_k = 1 \tag{4}$$

For steady-state conditions, the above system of balance equations is transformed in a form suitable for a numerical integration. Steady-state conditions imply that time derivatives equal zero, $\partial / \partial t = 0$. The left hand side convection term in Eq. (3) is differentiated, and it is obtained

$$h_k \frac{\mathrm{d}(\alpha_k \rho_k u_k)}{\mathrm{d}x} + \alpha_k \rho_k u_k \frac{\mathrm{d}h_k}{\partial x} = M_{2n+k}, \quad k = 1, n \tag{5}$$

Substituting the mass balance equation (1) into (5) the equation for enthalpy calculation is obtained

$$\frac{\mathrm{d}h_k}{\mathrm{d}x} = \frac{M_{2n+k} - h_k M_k}{\alpha_k \rho_k u_k} \tag{6}$$

Differentiation of the convection term in Eq. (1) and multiplication of Eq. (1) with the fluid velocity gives

$$\alpha_k \rho_k u_k \frac{\mathrm{d}u_k}{\mathrm{d}x} + \rho_k u_k^2 \frac{\mathrm{d}\alpha_k}{\mathrm{d}x} + \alpha_k u_k^2 \frac{\partial \rho_k}{\partial p} \frac{\mathrm{d}p}{\mathrm{d}x} +$$

$$+\alpha_k u_k^2 \frac{\partial \rho_k}{\partial h_k} \frac{\mathrm{d}h_k}{\mathrm{d}x} = u_k M_k \tag{7}$$

while differentiation of Eq. (2) leads to

$$2\alpha_k \rho_k u_k \frac{\mathrm{d}u_k}{\mathrm{d}x} + \rho_k u_k^2 \frac{\mathrm{d}\alpha_k}{\mathrm{d}x} + \alpha_k u_k^2 \frac{\partial \rho_k}{\partial p} \frac{\mathrm{d}p}{\mathrm{d}x} +$$

$$+\alpha_k u_k^2 \frac{\partial \rho_k}{\partial h_k} \frac{\mathrm{d}h_k}{\mathrm{d}x} + \alpha_k \frac{\mathrm{d}p}{\mathrm{d}x} = M_{n+k} \tag{8}$$

The velocity derivative is expressed from Eq. (7) as

$$\frac{\mathrm{d}u_k}{\mathrm{d}x} = \frac{u_k M_k - \rho_k u_k^2 \frac{\mathrm{d}\alpha_k}{\mathrm{d}x} - \alpha_k u_k^2 \frac{\partial \rho_k}{\partial p} \frac{\mathrm{d}p}{\mathrm{d}x} - \alpha_k u_k^2 \frac{\partial \rho_k}{\partial h_k} \frac{\mathrm{d}h_k}{\mathrm{d}x}}{\alpha_k \rho_k u_k} \tag{9}$$

Substitution of Eq. (9) in Eq. (8) leads to

$$\frac{\mathrm{d}\alpha_k}{\mathrm{d}x} = \alpha_k \frac{1 - u_k^2 \frac{\partial \rho_k}{\partial p}}{\rho_k u_k^2} \frac{\mathrm{d}p}{\mathrm{d}x} -$$

$$-\frac{M_{n+k} - 2u_k M_k + \alpha_k u_k^2 \frac{\partial \rho_k}{\partial h_k} \frac{\mathrm{d}h_k}{\mathrm{d}x}}{\rho_k u_k^2} \tag{10}$$

Table 1. Source terms in the balance equations (1-3) for bubbly or transitional (churn or slug) flow

- Number of fluid streams: $n = 2$
- Fluid streams indexes: $k = 1$ – gas,
$\quad\quad\quad\quad\quad\quad\quad\quad\; k = 2$ – liquid.

Mass balance source terms

Gas flow

$$M_1 = \Gamma_{21} - \Gamma_{12} \tag{T1-1}$$

Liquid phase

$$M_2 = \Gamma_{12} - \Gamma_{21} \tag{T1-2}$$

Momentum balance source terms

Gas flow

$$M_3 = -a_{21}\tau_{21} - a_{1W}\tau_{1W} + \Gamma_{21}u_2 - \Gamma_{12}u_1 - \alpha_1\rho_1 g \sin\theta \tag{T1-3}$$

Liquid phase

$$M_4 = a_{21}\tau_{21} - a_{2W}\tau_{2W} + \Gamma_{12}u_1 - \Gamma_{21}u_2 - \alpha_2\rho_2 g \sin\theta \tag{T1-4}$$

Energy balance source terms

Gas flow

$$M_5 = (\Gamma_{21} - \Gamma_{12})h'' + \dot{Q}_1 \tag{T1-5}$$

Liquid phase

$$M_6 = (\Gamma_{12} - \Gamma_{21})h'' + \dot{Q}_2 \tag{T1-6}$$

Equation (10) is written for all fluid streams involved in two-phase flow pattern, i.e. for k=1, 2,...n, and these equations are summed. Introducing the differential form of Eq. (4)

$$\sum_{k=1}^{3} \frac{\mathrm{d}\alpha_k}{\mathrm{d}x} = 0 \tag{11}$$

into the sum of Eq. (10) for every fluid, the following equation for the pressure calculation is obtained

$$\frac{\mathrm{d}p}{\mathrm{d}x} = \frac{\displaystyle\sum_{k=1}^{n} \frac{M_{n+k} - 2u_k M_k + \alpha_k u_k^2 \frac{\partial \rho_k}{\partial h_k}\frac{\mathrm{d}h_k}{\mathrm{d}x}}{\rho_k u_k^2}}{\displaystyle\sum_{k=1}^{3} \alpha_k \frac{1 - u_k^2 \frac{\partial \rho_k}{\partial p}}{\rho_k u_k^2}} \tag{12}$$

The final set of balance equations is derived in the form of Eqs. (6), (9), (10) and (12). These equations are written for every fluid stream involved in the modelled two-phase flow pattern. This form of derived equations is suitable for the direct application of a numerical integration method. In this investigation, the Runge-Kutta method is applied. The derivates are calculated in the order that first the enthalpy derivative is calculated from Eq. (6). Than, the pressure derivative is calculated

from Eq. (12) by using the result of Eq. (6). Equation (10) is calculated by using the solutions from (6) and (12) and finally, the derivative in Eq. (9) is calculated by using the results of previous three Eqs. (6), (10) and (12). The numerical simulation of the two-phase flow represents the solution of the Cauchy problem, where the initial conditions are defined flow parameters (dependent variables $\alpha_{k,0}$, $u_{k,0}$, $h_{k,0}$, p_0) at the inlet of the flow channel (initial value of independent variable being $x_0 = 0$).

2.2 Closure Laws

A set of closure laws is required for the calculation of mass, momentum and energy interface transfer processes for each of the modelled flow pattern. A detailed presentation of all necessary closure laws would exceed the content of this paper, hence, as an illustration, the closure laws for the bubbly flow are presented in Table 2. The detailed presentation of used closure laws is given in [6,18,19,20]. Evaporation and condensation rates in all flow patterns are calculated using thermal non-equilibrium models. The wall heat flux is prescribed according to the simulated experimental conditions and the heat is transferred from the wall to the liquid phases that are in contact to the wall.

Table 2. Closure laws for bubbly flow

	Bubbly flow	
Constitutive correlation	Pipe flow	Annulus flow
Wall-fluid area concentration	$a_{kW} = \dfrac{4\alpha_k}{D_h}$, $k=1,2$, $D_h = \dfrac{4A}{S}$, [18] (T2-1)	
	$A = \pi D^2/4$, $S = \pi D$	$A = \pi(D_2^2 - D_1^2)/4$, $S = \pi(S_1 + S_2)$
Wall shear stress	$\tau_{kW} = f_{kW} \dfrac{\rho_k \lvert u_k \rvert u_k}{2}$, $k=1,2$, [18] (T2-2) $f_{kW} = \dfrac{C}{Re_k^n}$ For turbulent flow $C = 0.079$, $n = 0.25$ For laminar flow $C = 16$, $n = 1$. $Re_k = \dfrac{\rho_k u_k D_h}{\mu_k}$	
Liquid-gas interfacial area concentration	$a_{21} = 6\dfrac{\alpha_1}{D_B}$ (T2-3) $D_{B,\max} = 31,68 D_h^{2/5}\left(\dfrac{\sigma}{\rho_1}\right)^{3/5}\left(\dfrac{\rho_1}{\rho_2}\right)^{1/5} u_m^{6/5}$, [11,19] $D_B = 0.0615 D_{B,\max}$ $u_m = (\alpha_1\rho_1 u_1 + \alpha_2\rho_2 u_2)/\rho_m$ $\rho_m = \alpha_1\rho_1 + \alpha_2\rho_2$	
Interfacial shear stress	$\tau_{21} = \dfrac{1}{8}\rho_2 f_{21}\lvert u_1 - u_2\rvert(u_1 - u_2)$ (T2-4) $f_{LG} = \dfrac{24}{Re_B}(1 + 0.15 Re_B^{0.687}) + \dfrac{0.42}{1 + 4.25\cdot10^4\, Re_B^{-1.16}}$, [4] $Re_B = \dfrac{\lvert u_1 - u_2\rvert D_B \rho_2}{\mu_2}$	
Subcooled boiling	$\Gamma_{21} = G\dfrac{dX_1}{dx}$, [10] (T2-5) $X_1 = X_{eq} - X_I \exp\left(\dfrac{X_{Geq}}{X_I} - 1\right)$ $X_{Geq} = \dfrac{h_{in} + 4\dot{q}_W x/(GD) - h'}{h_1 - h_2}$ $St\,\dfrac{\dot{q}_w}{0.88\cdot10^7} = 0.0065$ for $Pe > 70000$ $Nu\,\dfrac{\dot{q}_w}{0.88\cdot10^7} = 455$ for $Pe < 70000$ $St = \dfrac{\dot{q}_w}{Gc_{p2}(T_{sat} - T_2)}$, $Nu = \dfrac{\dot{q}_w D}{k_2(T_{sat} - T_2)}$, $Pe = \dfrac{GDc_{p2}}{k_2}$, $X_I = \dfrac{c_{p2}(T_2 - T_{sat})}{h_1 - h_2}$, $G = \sum_{k=1}^{2}\alpha_k\rho_k u_k$	
Saturated boiling	$\Gamma_{21} = \dfrac{1}{\tau_e}\dfrac{h_2 - h'}{h'' - h'}$ (T2-6)	

The mist flow pattern is considered after the depletion of liquid films in the annular flow. The gas phase interaction in mist flow with the wall is calculated as in the bubbly flow, while the droplets interface processes are calculated as in annular flow pattern, and the heat is transferred from the wall directly to the droplets. In case of all droplets evaporation, the one phase vapour flow is calculated. As the trivial situations (regarding the two-phase flow conditions) one-phase liquid and vapour flows are not described here, and they are treated as the limiting condition of bubbly flow when either vapour volume fraction or liquid volume fraction equals zero. The re-establishment of the annular flow from the mist flow is defined by the criteria that the droplets deposition rate overrides the evaporation rate of all deposited droplets. Transitions from the bubbly to churn flow and from churn to annular flow pattern have been predicted according to the modified Bennett flow-pattern map described in [11], Fig. 2.

For annular flow, it is adopted that the dry-out occurs when the complete liquid film depletion happens. The complete film disappearance is triggered at the

minimum possible film thickness, which is determined by the complex effects of annular flow conditions, such as droplets entrainment and deposition, hydrodynamic stability of liquid film surface waves, bubble nucleation and bursting on the wall surface, etc. For adiabatic water-air atmospheric flow within experimental rod bundle, the minimum liquid film thickness was predicted to be 100 microns [13]. The film on the heated wall should be of the smaller minimum thickness. In [17] it was experimentally and theoretically predicted that the minimum film thickness under saturated pool boiling conditions is in the range from 2 to 10 microns. Numerical results on stable minimum film thickness, but not close to the dry-out conditions, are reported to be as low as 35 microns [2]. These previous results show that the minimum possible film thickness, prior to the dry-out triggering are in the range of several microns. In this paper, the minimum possible film thickness at the onset of dry-out is assumed to be equal or less than 4 microns.
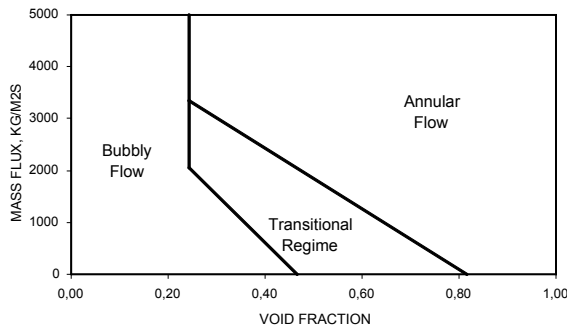

Figure 2. Modified Bennett's map for steam-water upward flow in a pipe at 7 MPa [11].

Presented methodology is applied to the simulation and analyses of the boiling water tube with dry-out at the channel exit, as well as of the critical two-phase flow of hot liquid with adiabatic evaporation. Simultaneously, one-fluid, two-fluid and three-fluid models are solved for the calculation of one-phase, bubbly and churn flow, and annular flow with entrained droplets, respectively. In order to estimate the reliability of the applied multi-fluid model, some separate effects are analysed first, pertinent to the bubbly flow, churn and annular flow.

3. RESULTS AND DISCUSSIONS

3.1 Bubbly flow separate tests

Experimental data on upward bubbly flows in vertical pipes are analysed [19]. Two models are applied to the liquid-gas interfacial momentum transfer prediction: a topological model (TM), based on the bubble mean diameter, interfacial area concentration and bubble interfacial drag, as well as Dispersed Particle Model (DPM) based on the correlation for the interfacial drag momentum transfer between dispersed bubbles and continuous liquid phase [9]. The bubbly flow anomaly is stated. It is caused by the spatial cross sectional distribution of the gas phase void fraction, and it shows that the liquid cross-sectional averaged velocity is higher than the bubbles averaged velocity for higher

liquid superficial velocities. An empirical function of liquid superficial velocity is introduced in order to correct the liquid-gas interfacial shear stress in one-dimensional two-fluid model for cases of bubbly flow anomaly. The standard one-dimensional bubbly flow models, widely applied in the industry, are not able to predict the bubble flow anomaly, while the proposed improved bubbly flow model, shows acceptable accuracy in void fraction predictions [19].

Results of the one-dimensional two-fluid model predictions for bubbly flow are shown in Figs. 3 and 4. Favourable agreement of calculated data with the measured ones is obtained. There is no practical difference between the void fraction predictions performed with the Topological Model (TM) and Dispersed Particle Model (DPM) for interfacial drag. Void fraction predictions for the liquid superficial velocities higher or equal to 0.5 m/s are close to the homogeneous model predictions, while the homogeneous model highly over-predicts void fractions in bubbly flows with lower liquid superficial velocities.

3.2 Churn flow separate tests

Transitional flows between bubbly flows and annular flows are characterized by irregular gas-liquid interface shapes, whose length scales are difficult to be defined. Three multi-fluid modelling approaches are applied to transitional flows: topological bubbly flow model (BFM), transitional model (TM) based on the interfacial drag correlation for transitional flows, and model based on the interpolation of bubbly flow and annular flow interfacial transfer terms (IM), [20]. Performed is the simulation of air-water vertical upward flows in the circular tube of 0.0254 m inner diameter and the length of 1.5 m (Rose and Sewell experiment, reported in [7]). Experimental data and modelling predictions are presented in Fig. 5. According to the experimental data, the incipient of the transition flow starts when the measured void fraction starts to diverge from the homogeneous model prediction. The boundary void fraction value for the transitional flow incipient is 0.243, what is in agreement with the prediction of the modified Bennett two-phase flow map. The transition toward annular flow pattern is assumed at the void fraction value of 0.7. Figure 5 shows that the BFM is not able to predict the transitional flow. Due to the strong coupling between the phases in the bubbly flow model, it gives practically the same results as the homogeneous model which is based on the assumption that liquid and gas phase velocities are equal. The interpolation model (IT) predicts transitional flow void fraction fairly well. This is achieved by the IT model interpolation of the interfacial terms between the strongly coupled bubbly flow and the weakly coupled annular flow. Obviously, the transitional flow model is becoming less coupled with the void fraction increase. This also means that the transitional flow length scale increases and the interfacial area concentration decreases with the void fraction increase. The best agreement between calculated and measured data is obtained using the TM model.

3.3 Annular flow separate tests

Predictions of the boiling crisis in high quality regions of two-phase flows are the most sensitive to the accuracy of the annular flow modelling. Correlations for droplets entrainment and deposition and for liquid film-gas core interfacial friction have the greatest influence on the accuracy of annular flow modelling results. Several available correlations for droplets entrainment and deposition were tested and a matrix of results was obtained [18] for the condition of Gill-Hewitt experiment [8] of developing annular flow. Figures 6 and 7 show entrained droplets mass flux and liquid film thickness predicted using various entrainment correlations. A considerable discrepancy between predictions by different correlations is observed. The closest agreement is achieved by the correlation based on the Hutchinson&Whalley experimental data for entrainment.

3.4 Integral boiling channel simulation with CHF prediction

On the basis of the separate effect tests results, the appropriate models for the bubbly flow, churn flow and annular flow are chosen within the multi-fluid modelling approach and applied to the simulation of the water boiling channel with a dry-out in a high quality region. Simulations are performed for Kawara et al experimental data [10] and the AERE-R 5373 [3] experimental conditions. These are high pressure data and for them it is shown that the most appropriate combination of correlations consist of Sugawara correlations for droplets entrainment and deposition and Moeck correlation for liquid film-gas interfacial friction coefficient. Transitions from the bubbly to churn flow and from churn to annular flow pattern are predicted according to the Bennett flow-pattern map. At the incipient of annular flow it is assumed that 90% of liquid volume fraction continues to flow in the form of wall liquid film, while the rest of 10% forms entrained droplets. This assumption is empirical and it is prescribed by sensitivity studies in the process of CHF calculations. The best results were obtained by this ratio of liquid flow slip between liquid film and droplets flow at the location of annular flow incipient. The same ratio was determined in [15]. The initial velocities of entrained droplets and liquid film at the transition to annular flow, from churn or directly from bubbly flow, are prescribed to be the same. This is assumed to be physically realistic in one-dimensional modelling approach of transition to annular flow. In [15] it was assumed that at the incipient of annular flow the droplets velocity is 0.9 of gas phase velocity. But, this abrupt change of velocity of a portion of liquid volume leads to unrealistic change of the liquid stream momentum.

Predicted void fraction changes along the boiling flow channels are shown in Figs. 8 and 9. Much higher initial void fraction of entrained droplets is seen in Fig. 9. This is caused by an intensive droplets entrainment at the incipient of annular flow for flow conditions presented in Fig. 9. The transition from churn to annular

flow in this case occurs at low gas phase volume fraction and high liquid volume fraction. Initial thick liquid film leads to high rate of entrainment and abrupt increase of entrained droplets volume fraction.

The critical heat flux values are predicted with acceptable accuracy, Fig. 10. The criterion for the dry-out occurrence, in all performed simulations, is the wall liquid film thickness in the range from 4 to 5 μm. The other flow parameters, such as liquid film volume fraction or the rate of the liquid film mass flow to the total liquid mass flow, were not found appropriate to be used as the criterion for dry-out conditions, because of their high range of relative change within performed simulations. This example shows that schematisation of the multi-fluid approach gives sound bases for the definition of various criteria for two-phase flow effects prediction. The methodology enables quantification of relevant parameters of process involved two-phase flow streams, which serves as the basis for the derivation of required criteria for boiling crises.

Differences between measured and predicted critical thermodynamic qualities at the locations of dry-out are shown in Fig. 11. By comparing Figs. 10 and 11 it can be seen that critical qualities are predicted with less accuracy than CHFs. This means that the prediction of quality is more sensitive to the intensities of annular flow processes, such as droplets entrainment and deposition or liquid film-gas interface friction.

3.5 Critical two-phase flow test with adiabatic evaporation

Conditions of two-phase critical pipe flows, performed within the Super Moby Dick experimental research [14], are simulated using the multi-fluid model.

Vapour generation rate in adiabatic conditions is predicted by analytical correlations derived under the assumptions of conduction controlled heat transfer from the bulk liquid to the gas-liquid interface and convection controlled heat transfer [22]. Also, semi-empirical correlation for vapour generation is applied, based on the evaporation coefficient experimentally derived as a function of pressure [6]. Figure 12 shows a comparison of calculated and measured vapour generation rates. Calculated and measured pressures are compared in Fig. 13. Good prediction results were also obtained for the range of pressures at 20, 40, 80 and 120 bars.
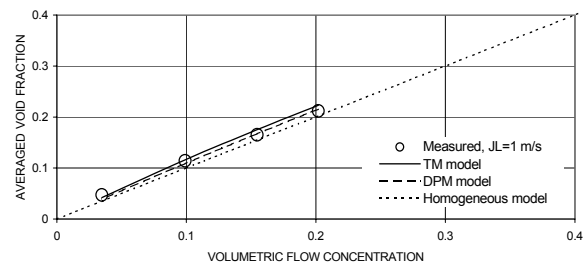

Figure 3. **Comparison of calculated and measured void fractions for different volumetric flow concentrations** $\beta = J_G /(J_L + J_G)$ **of Bensler's experiment [5]. Void fraction values are in all cases higher than the corresponding volumetric flow concentrations, indicating that the mean liquid velocity is higher than the mean bubbles velocity.**
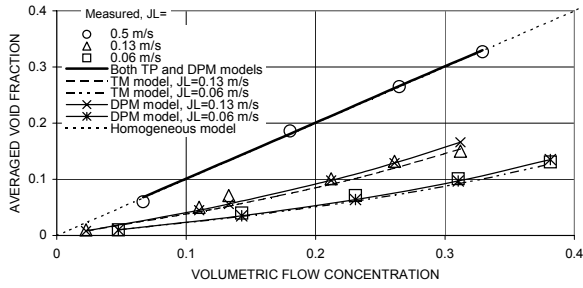
Figure 4. Comparison of calculated and measured void fractions for different volumetric flow concentrations of Bensler's experiment [5]. Measured and void fractions calculated with the TM and DPM models coincide with the homogeneous model prediction for J_L=0.5 m/s, indicating that the mean liquid and bubble velocities are equal. For lower J_L values void fractions are lower than corresponding volumetric flow concentrations, because the bubble mean velocity is higher than the liquid mean velocity.
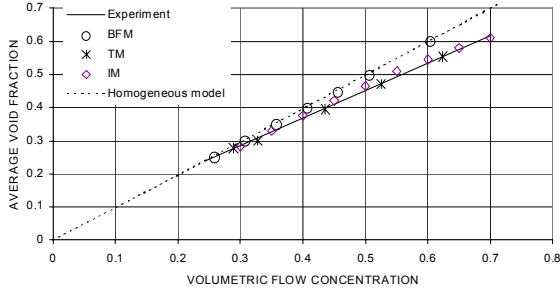
Figure 5. Comparison of measured and calculated average void fraction data α_G for different steam volumetric flow concentrations $\beta = J_G/(J_L + J_G)$ in transitional two-phase flow pattern. Homogeneous model over-predicts void fraction. Bubbly flow model (BFM) gives too high coupling between liquid and gas phase. Transitional model (TM) agrees well with experimental data. Calculation based on the interpolation between bubbly flow and annular flow parameters – Interpolation model (IM) represents fairly well experimental conditions [20].
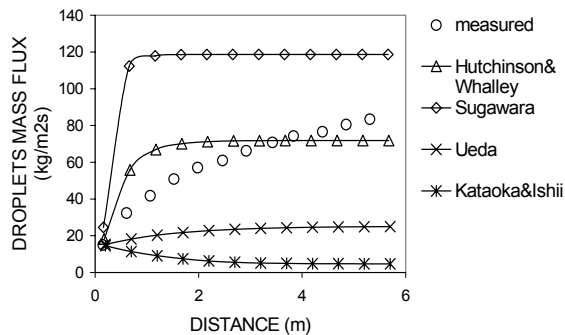

Figure 6. Entrained droplets flow rate predicted with the multi-fluid model and various correlations for droplets entrainment (simulation of the Gill-Hewitt experiment at nearly atmospheric conditions, [8]). Deposition rate is calculated with constant deposition coefficient k_D=0.15.
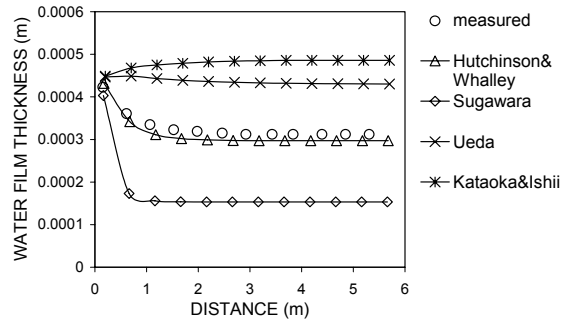

Figure 7. Film thickness predicted with the multi-fluid model and various correlations for droplets entrainment (simulation of the Gill-Hewitt experiment at nearly atmospheric conditions, [8]). Deposition rate is calculated with constant deposition coefficient k_D=0.15.
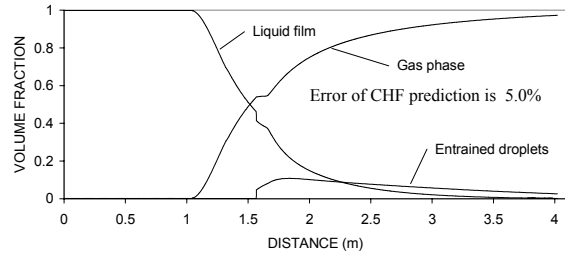

Figure 8. Void fraction prediction for the critical heat flux flow conditions [10]. The test parameters are p=5 MPa, D=10 mm, L=4.02 m, G=1500 kg/m^{2}s, Δh_{sub}=460 kJ/kg. Heat flux is uniform. The results are obtained by the combination of the Sugawara correlations for entrainment and deposition. Experimental value of the critical heat flux is 1274 kW/m^2, while the calculated value is 1210 kW/m^2.
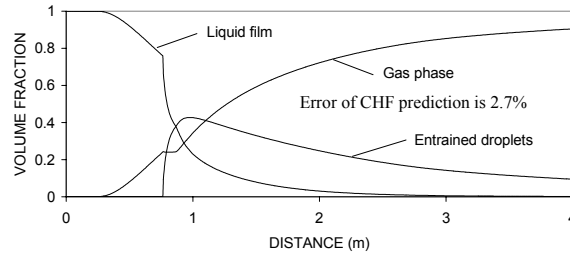

Figure 9. Void fraction prediction for the critical heat flux flow conditions (AERE-R 5373 test data [3]). The test parameters are p=6.89 MPa, D=12.6 mm, $L_{boiling}$=3.72 m, G=1980 kg/m^{2}s, Δh_{sub}=19.8 kJ/kg. Heat flux is uniform. The results are obtained by the combination of the Sugawara correlations for entrainment and deposition [21]. Experimental value of the critical heat flux is 1070 kW/m^2, while the calculated value is 1100 kW/m^2.
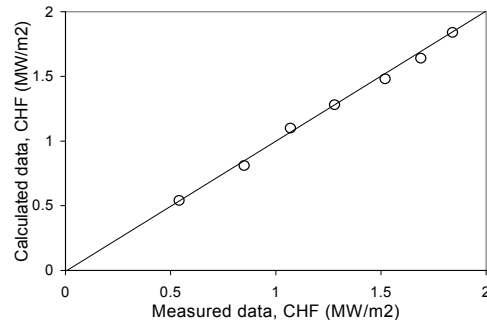

Figure 10. Predictions of CHFs for AERE-R experimental conditions [3]. Test parameters are p=6.89 MPa, D=12.6 mm, G=400÷5200 kg/m2s, ΔT_{sub}=10÷350°C. Heat flux is uniform.
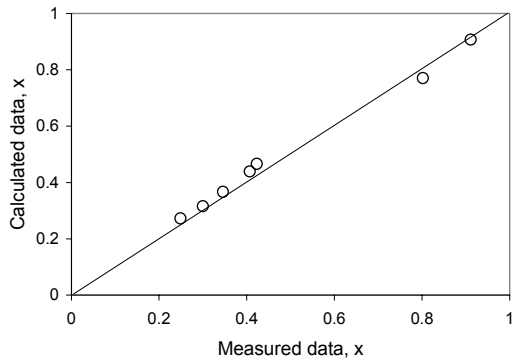
Figure 11. Predictions of thermodynamic qualities for AERE-R experimental conditions [3]. Test parameters are *p*=6.89 MPa, *D*=12.6 mm, *G*=400÷5200 kg/m²s, ΔT_sub=10÷35⁰C. Heat flux is uniform.
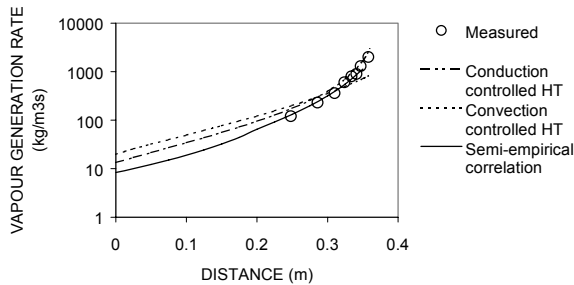

Figure 12. Comparison of multi-fluid model predicted and measured vapour generation rates for critical two-phase flow of Super Moby Dick experiment at 20 bars [14].
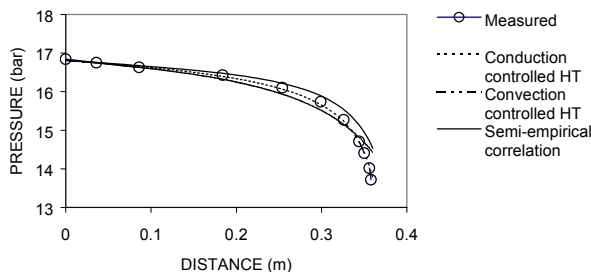

Figure 13. Comparison of multi-fluid model predicted and measured pressure change for critical two-phase flow of Super Moby Dick experiment at 20 bars [14].

4. CONCLUSIONS

The multi-fluid modelling approach is presented. It is applied to the simulation of hydrodynamic separate effect tests for bubbly, churn and annular flow. It is stated that the accuracy of the bubbly and churn-turbulent flow prediction strongly depends on the prediction of the interfacial momentum transfer due to the interfacial drag, while annular flow prediction is the most sensitive to the prediction of the droplets entrainment and deposition and liquid-film gas core interfacial friction. Also, the methodology is applied to the prediction of two-phase critical flow with adiabatic evaporation of superheated liquid. The methodology is also used for the simulation of the water boiling channel with dry-out occurrence in the annular flow region at the pipe exit. The prediction of the critical heat flux is performed with the acceptable accuracy.

NOMENCLATURE

A	- channel cross-sectional area [m²]
a	- interfacial area concentration [m⁻¹]
C_p	- specific heat [J/kgK]
D	- pipe diameter [m]
D_1	- diameter of the annulus inner wall [m]
D_2	- diameter of the annulus outer wall [m]
f	- friction coefficient
g	- gravitational constant [m/s²]
h	- enthalpy [J/kg]
J	- superficial velocity, $J_k = \alpha_k u_k$
k	- heat conduction coefficient [W/mK]
M	- source terms in balance equations
$\dot{m}$	- mass flow rate [kg/s]
n	- number of fluid streams
Nu	- Nusselt number
p	- pressure [Pa]
Pe	- Peclet number
$\dot{q}_w$	- heat flux [W/m²]
$\dot{Q}$	- volumetric heat rate [W/m³]
Re	- Reynolds number
Re_B	- bubble Reynolds number,
S	- perimeter [m]
St	- Stanton number
T	- temperature [K]
u	- velocity [m/s]
X	- quality
x	- coordinate [m]
W_d	- deposition rate of entrained droplets [kg/m²s]
W_e	- droplets entrainment rate [kg/m²s]

Greek letters:

Γ	- evaporation/condensation rate [kg/m³s]
α	- volume fraction
δ	- liquid film thickness, [m]
θ	- angle of flow channel inclination
μ	- dynamic viscosity [kg/ms]
ρ	- density [kg/m³]
τ	- friction shear stress [N/m²]
τ_e	- evaporation relaxation time [s]

Subscripts:

h	- hydraulic parameter
k	- phase indicator,

REFERENCES

[1] Alipchenkov, V.M., Nigmatulin, R.I., Soloviev, S.L., Stonik, O.G., Zaichik, L.I., Zeigarnik, Y.A.: A three-fluid model of two-phase dispersed-annular flow, International Journal of Heat and Mass Transfer 47, pp. 5323-5338, 2004.

[2] Antal, S. P., Nagrath, S., Podowski, M. Z.: On the Multidimensional Modeling of Annular Two-Phase Flows around Spacers, Proceedings of the 4th International Conference on Multiphase Flow (on CD), New Orleans, paper 167, USA, 2001.

[3] Bennet, A.W., Hewitt, G.F., Kearsey, H.A., Keeys, R.K.F.: Heat transfer to steam-water mixtures flowing in uniformly heated tubes in which the critical heat flux has been exceeded, Report AERE-R-5373, 1967.

[4] Clift, R., Grace, J.R., Weber, M.E.: *Bubbles, Drops and Particles*, Academic Press, New York, 1978.

[5] Delhaye, J. M., Bricard, P.: Interfacial Area in Bubbly Flow: Experimental Data and correlations, Nuclear Engineering and Design, 151, pp. 65-77, 1994.

[6] Galic, N., Stevanovic, V.: A Numerical Simulation of Two-Phase Critical Flow, Termotehnika-Journal of the Yugoslavian Society of the Heat Transfer Engineers, 21, pp. 53-61, 1995.

[7] Griffith, P.: Characteristics of Bubbly Flow, Proceedings of the 2nd International Workshop on Two-Phase Flow Fundamentals, Rensselaer Polytechnic Institute, Data Set No. 2, Troy NY, 1987.

[8] Hewitt, G. F.: Developing Annular Flows, Proceedings of the 2nd International Workshop on Two-Phase Flow Fundamentals, Rensselaer Polytechnic Institute, Data Set No. 3, Troy NY, 1987.

[9] Ishii, M., Zuber, N.: Drag Coefficient and Relative Velocity in Bubbly, Droplet or Particulate Flows, AIChE Journal, 25, pp. 843-855, 1979.

[10] Kawara, Z., Kataoka, I., Serizawa, A., Ko, Y. J., Takahashi, O.: Analysis of Forced Convective CHF Based on Two-Fluid and Three-Fluid Model, Proceedings of the 11th IHTC, 2, pp. 103-108, 1998.

[11] Kuznecov, Yu. N.: *Heat Transfer in Problems of the Nuclear Reactors Safety*, Energoatomizdat, Moscow, (in Russian), 1989.

[12] Lee, S.I., No, H.C.: Assessment of an entrainment model in annular-mist flow for a three-field TRAC-M, Nuclear Engineering and Design 237, pp. 441-450, 2007.

[13] Noriyasu, K., Kumagai, K., Tsuji, Y., Kunugi, T., Serizawa, A.: Multi-dimensional Characteristics of Surface Waves on the Liquid Film Flow in a 3x3 Rod Bundle, Proceedings of the 4th International Conference on Multiphase Flow (on CD), New Orleans, USA, paper 912, 2001.

[14] Reocreux, M.: Flashing flow, Proceedings of the 2nd International Workshop on Two-Phase Flow Fundamentals, Rensselaer Polytechnic Institute, Data Set No. 13, Troy NY, 1987.

[15] Saito, T., Hughes, D.D., Carbon, M.W.: Multi-fluid modeling of annular two-phase flow, Nuclear Engineering and Design 50, pp. 225-271, 1978.

[16] Sami, S.M.: An improved numerical model for annular two-phase flow with liquid entrainment, International Communication in Heat and Mass Transfer 15, pp. 281-292, 1988.

[17] Serizawa, A.: Theoretical Prediction of Maximum Heat Flux in Power Transients, International Journal of Heat and Mass Transfer, Vol. 26, pp. 921-932, 1983.

[18] Stevanovic, V., Studovic, M.: A simple model for vertical annular and horizontal stratified two-phase flows with liquid entrainment and phase transitions: one-dimensional steady state conditions, Nuclear Engineering and Design 154, pp. 357-379, 1995.

[19] Stosic, Z., Stevanovic, V.: A Comparative Analysis of Bubbly Flow Parameters Based on Different Approaches for Interfacial Drag, Proceedings of the 5th World Conference on Experimental Heat Transfer, Fluid Mechanics and Thermodynamics, pp. 1393-1400, Thessaloniki, Greece, 2001.

[20] Stosic, Z., Stevanovic, V.: Prediction Methods for Interfacial Drag in Transitional Two-Phase Flow Regimes, Proceedings of the 5th World Conference on Experimental Heat Transfer, Fluid Mechanics and Thermodynamics, pp. 1459-1464, Thessaloniki, Greece, 2001.

[21] Sugawara, S.: Droplet deposition and entrainment modelling based on the three-fluid model, Nuclear Engineering and Design 122, pp. 67-84, 1990.

[22] Vernier, Ph., Berne, Ph.: An Appraisal of Interfacial Vapour Generation Laws Used in Thermal hydraulic Analysis, The Second Int. Topical Meeting on Nuclear Reactor Thermal-Hydraulics, Santa Barbara, USA, pp. 310-315, 1983.

[23] Wallis, G.B.: *One-Dimensional Two-Phase Flow*, McGraw-Hill, New York, 1969.

СИМУЛАЦИЈА ДВОФАЗНОГ СТРУЈАЊА ГАС-ТЕЧНОСТ У ВЕРТИКАЛНОЈ ЦЕВИ ПРИМЕНОМ ВИШЕФЛУИДНОГ МОДЕЛА

Владимир Стевановић, Сања Прица, Блаженка Масловарић

Развијен је потпун, стабилан, једнодимензиони вишефлуидни модел за предвиђање двофазног струјања у вертикалним цевима. Модел је заснован на билансима одржања масе, количине кретања и енергије, који су примењени на сваку флуидну струју која је присутна у посматраном облику двофазног струјања, као и на одговарајућим конститутивним корелацијама за одређивање транспортних процеса на разделним површинама између фаза. Билансне једначине за стационарно стање су трансформисане у облик погодан за директну примену нумеричке методе за интеграцију система обичних диференцијалних једначина. Симулирани су термохидраулички процеси дуж целог испаривачког канала, почевши од струјања и загревања потхлађене течности на улазу у струјни канал па до засушења течног филма и појаве магленог тока са капима укљученим у гасну фазу на крају канала. Такође, модел је тестиран и за услове неколико парцијалних ефеката двофазног струјања.